Construction and Building Materials 458 (2025) 139512

Contents lists available at ScienceDirect

Construction and Building Materials

journal homepage: www.elsevier.com/locate/conbuildmat

Novel soybean dregs biochar concrete: Characterization and evaluation of the mechanical properties and microstructure

Shujie Liu [a], Zheng Chen [a,*], Jie Shao [a], Shujian Luo [a], Deliang Yu [b]

[a] School of Materials Science and Engineering, Xi'an University of Architecture and Technology, Xi'an, Shaanxi Province 710055, China
[b] Engineering Quality Inspection Department, China Design Group Co., Ltd, Nanjing, Jiangsu Province 210001, China

ARTICLE INFO

Keywords:
Soybean dregs
Biochar concrete
Mechanical property
Microstructure

ABSTRACTS

Soybean dregs produced by the soybean processing industry were agricultural waste with significant treatment costs. To explore economical and efficient treatment methods, this study used pyrolysis technology to convert soybean dregs into biochar with resource utilization value. Soybean dregs biochar was applied to concrete to research the impacts of different incorporation methods and dosages on concrete properties. The physical properties of soybean dregs biochar after pyrolysis at various temperatures were characterized using Brunauer-Emmett-Teller (BET), X-ray diffraction (XRD), Fourier transforms infrared spectrometer (FTIR), and Scanning electron microscope (SEM). The influences of soybean dregs biochar on the mechanical properties and microstructure of concrete were analyzed. The results revealed that soybean dregs exhibited a rich pore structure and a large specific surface area after pyrolysis at high temperatures, which effectively filled the internal pores of concrete and enhanced the compactness of the paste structure. Regardless of the incorporation method, the mechanical properties improved with a biochar content of 2 %-4 % compared to the control group. However, as the content increased further, the mechanical properties of concrete began to exhibit a decreasing trend. Furthermore, replacing 3 % of sand with biochar in concrete demonstrated the greatest improvement in mechanical properties, surpassing the effects of replacing cement or acting as a filler. This substitution resulted in a 12.32 % increase in compressive strength and a 16.42 % increase in tensile strength.

1. Introduction

China is a major consumer of soybeans, and the rapid development of the soybean processing industry has led to a sharp increase in the production of soybean dregs. According to statistics, the current domestic soybean food industry produces about 20 million tons of soybean dregs per year. The water content of soybean dregs is around 80–90 %, making it susceptible to spoilage and not conducive to transportation and storage[1]. Therefore, only a very small portion is used as feed fertilizer, while the majority of the soybean dregs are directly landfilled or incinerated as solid garbage[2], causing an environmental problem of wasted resources. Finding ways to realize the comprehensive utilization of soybean dregs resources and solve environmental problems has become a hot topic and trend in current research. Since soybean dregs are rich in fiber and protein, it is possible to obtain biochar from soybean dregs by pyrolysis at high temperatures under oxygen-limited conditions. This not only reduces the cost of disposal but also increases its economic value in environmental management and realizes the resource utilization of waste.

Biochar is a porous material with stable properties, a large specific surface area, good biochemical properties, and thermal stability[3]. Its rich pore structure and high specific surface area made it highly adsorbent, leading to extensive applications in fields such as effluent treatment, heavy metal removal, and clean energy[4]. Soybean dregs are mainly modified into biochar as an adsorbent to remove harmful ions from the environment. Li[5]obtained soybean dregs biochar by pyrolysis at 800℃, resulting in an ion removal rate as high as 84.15 % after ball milling-assisted potassium hydroxide activation. Shan[6]prepared biochar from soybean dregs and found that it had more micropores and larger specific surface area. High-temperature carbonization promoted the formation of aromatic groups and increased the crystallinity of the biochar making its structure more stable. Wang[7]prepared soybean dregs biochar by hydrothermal synergistic pyrolysis, indicating that it had a good specific surface area and a porous structure. These porous structures contained numerous nanochannels, providing abundant active sites for the adsorption process[8]. It was evident that

* Corresponding author.
E-mail address: chenz@xauat.edu.cn (Z. Chen).

https://doi.org/10.1016/j.conbuildmat.2024.139512
Received 2 August 2024; Received in revised form 5 December 2024; Accepted 6 December 2024
Available online 12 December 2024

soybean dregs biochar had a beneficial effect on pollutant removal. However, considering resource utilization, biochar obtained from soybean dregs must be modified and pretreated to improve its adsorption efficiency. Therefore, new treatment pathways are needed to achieve sustainable utilization of soybean dregs biochar.

Concrete is the most used and irreplaceable material in the construction sector due to its low cost and excellent performance, which results in concrete accounting for 7 % of global CO_2 emissions[9]. Therefore, replacing the use of construction materials with carbon-neutral materials in concrete production is a promising way to reduce CO_2 emissions. Many studies have shown that biochar has a high degree of chemical stability and is an ideal material for replacing various components of concrete[10]. Some of the biochar has a certain volcanic ash effect due to the presence of silica, which could improve the performance of concrete very well. In the production of biochar, only a small portion of the carbon was emitted in the form of carbon dioxide; more was stored inside and absorbed carbon dioxide in the air, so it had a good carbon sequestration effect[11]. Dixit[12]found that the fineness of biochar below 75 μm replaced sand because its finer particle size filled the voids well and had a positive effect on the early hydration rate, resulting in an increase in compressive strength of more than 50 %. D Suarez-Riera[13]found that wood biochar had some micro-reinforcement in cement pastes, which could improve the fracture properties of cement mortar. The flexural strength of cement mortar was increased by 15 % by adding 2 % biochar. Berti[14]found that biochar added as a filler formed a uniformly distributed network that bound with the cement to form a more stable structure and reduced porosity. Wang [15]pyrolyzed waste wood at temperatures of 500℃ and 700℃ to obtain biochar, found that the 700℃ pyrolysis of biochar helped to enhance the adhesion with the matrix. The content of biochar could promote the compressive strength as long as it was controlled within 5 %. However, when the content was too much, the compressive strength began to show a decreasing trend[16].

Although biochar could have a positive effect on the performance of concrete, the physicochemical properties of biochar are strongly influence by factors such as the source of biomass and the pyrolysis process. Existing biochar research mainly focus on wood and straw, and there is still relatively little research on soybean dregs biochar in the construction. Therefore, it is necessary to investigate the effect of soybean dregs biochar on concrete properties to fill the current research gap and to provide a theoretical basis for the application and dissemination of biochar concrete.

In this study, soybean dregs were cracked into biochar at different temperatures. The physical properties of soybean dregs before and after high-temperature pyrolysis were analyzed at the microscopic level. The effect of soybean dregs biochar as a replacement for cement, sand, and fillers on the workability, basic mechanical properties, and microstructure of concrete was investigated. The effect of biochar incorporation on the hydration reaction of cement and microstructural composition of concrete was analyzed.

2. Materials and methods

2.1. The selection of materials

Conch brand P.O 42.5 ordinary Portland cement was selected, and the chemical composition and physical properties were shown in Table 1 and Table 2. The fine aggregate was natural river sand with a continuous gradation. The coarse aggregate size ranged from 4.75mm to 20 mm.

Table 2
Physical characteristics of the cement.

W/C	S/C	Setting time (min)		Flexural strength (MPa)		Compressive strength (MPa)	
		Initial set	Final set	3 d	28 d	3 d	28 d
0.5	3.0	150	215	5.3	8.4	22.7	47.7

The water reducer used was polycarboxylate superplasticizer (SP) produced by Shaanxi KZJ New Materials Co., Ltd. The solid content was 10 %, and the water reduction rate was not less than 25 %. The experimental water used was tap water.

2.2. Preparation of soybean dregs biochar

In this study, soybean dregs (OA) were used as the raw material for biochar, and it was pyrolyzed under oxygen-limited conditions. The pyrolysis temperature was increased to 300℃, 500℃ and 700℃ at a heating rate of 15℃/min, and maintained at a constant temperature for 1.5 h to ensure complete carbonization (hereinafter referred to as 3BC, 5BC, 7BC). After natural cooling to room temperature, soybean dregs biochar (hereinafter referred to as BC) was ground, sifted through a 100-mesh sieve, and bagged in a dry place for backup. The physicochemical properties of OA after pyrolysis at different temperatures were analyzed using microscopic methods. Because the biochar pyrolyzed at 700℃ had a large specific surface area and a small pore size distribution, it could better exert the filling effect and enhance the adhesion to the matrix. Therefore, it was used as a substitute for concrete materials in subsequent experiments.

The particle size distribution of OA before and after pyrolysis was analyzed by laser particle size analyzer (Mastersizer 2000). The wet dispersion technology was used in the test, and ethanol was used as the dispersant for analysis. The particle size distribution of 7BC was shown in Fig. 1. The same technique was used to determine the distribution of cement particles for comparison (Fig. 1). Table 3 showed the particle

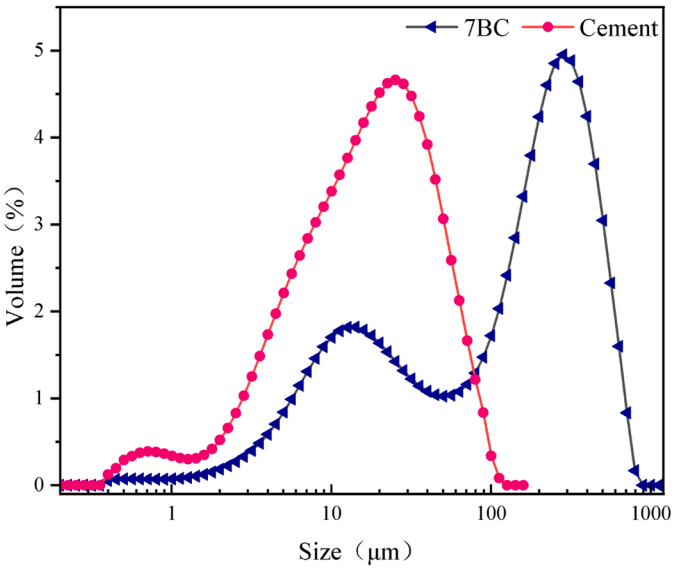

Fig. 1. Particle size distribution of 7BC and cement.

Table 1
Chemical composition of cement (wt%).

Composition	CaO	Al_2O_3	SO_3	Fe_2O_3	MgO	Na_2O	K_2O	SiO_2	LOI
Weight	62.28	5.67	2.63	4.13	1.83	0.36	0.14	21.08	1.61

Note: LoI (Loss on ignition)

Table 3
Particle size of biochar and cement at different cumulative percentages (μm).

	10 %	50 %	90 %
7BC	7.9	141.5	399.1
Cement	3.5	16.2	48.0

size of 7BC and cement when the cumulative percentage of particle size distribution was 10 %, 50 % and 90 %, respectively. It could be seen that about 90 % of the 7BC particles were below 0.40 mm, while about 50 % of the particles were below 0.14 mm. By comparing the particle size distribution of cement particles, it could be seen that although the particle size of 7BC was larger than that of cement particles, there were still some finer than cement particles. Scholars[17] had also shown that fine-grained fillers had more substantial benefits in cement hydration and fillers than coarse-grained fillers, and the incorporation of finer biochar could well exert its filling effect.

The elemental analysis of BC after pyrolysis at 700℃ was carried out by Elemantar Vario EL cube analyzer. The elemental composition of 7BC was shown in Table 4. It could be seen that the content of C element increased significantly and the content of O element decreased after pyrolysis. This indicated that dehydration, dehydroxylation, decarboxylation and other reactions occurred during the pyrolysis of OA, indicating the conversion of OA to carbon-rich materials.

2.3. Concrete ratios and preparation

According to the different mixing methods of BC, three concrete mix ratios were designed, as shown in Table 5. BC replaced cement with 2 %, 4 %, 6 %, and 8 % by weight (marked as A) and acted as a filler with an equal admixture (marked as B), while sand was replaced with 1 %, 2 %, 3 %, 4 %, and 5 % (marked as C). A total of 15 groups of concrete were designed, with the group without biochar serving as a blank control group. Mechanical properties were tested on three samples from each group at 28 d (Fig. 2).

During the preparation of the specimen, the aggregate, cement, and BC were poured into the stirring pot and stirred for 1 min. Then, the superplasticizer and water were slowly added for stirring for 5 min. The new mix was loaded into 100 mm × 100 mm × 100 mm and 100 mm × 100 mm × 400 mm molds coated with machine oil internally in three batches. Put it on the concrete vibration table and vibrated it until the cement paste appears on the surface and there were no obvious air bubble overflows. The surface was smoothed with a spatula until the difference between the surface of the mixture and the edge of the mold did not exceed 0.5 mm. The specimens were demolded after 24 h, and then placed in a standard curing room with 20 ± 2℃ and humidity of more than 95 % for 28 d.

2.4. Methods

2.4.1. Mechanical properties

The slump of concrete was measured according to the China standard GB/T 50080–2016. The compressive strength, splitting tensile strength, and flexural tensile strength of concrete at 28 d were determined according to the China standard GB/T 50081–2019. The compressive and tensile strength of concrete cubes with dimensions of 100 mm in side were determined using the DYE-2000 electro-hydraulic pressure tester. The flexural strength of concrete with dimensions of 100 mm × 100 mm × 400 mm was measured using the four-point bending method in the CMT5105 microcomputer-controlled electronic universal testing machine. In the measurement of the mechanical properties of concrete, the samples were loaded in a continuous uniform loading mode. The loading rate was 0.5 MPa/s for compressive strength tests and 0.05 MPa/s for tensile and flexural strength tests.

Table 4
Elemental analysis before and after OA pyrolysis (%).

	C	H	O	N
OA	45.84	6.63	43.78	3.75
7BC	78.6	1.91	14.84	4.65

Table 5
Mixing design of BC concrete (kg/m^3).

Mix code	Cement	Sand	Coarse aggregate	Water	SP	Biochar
P0	420	718	925	168	5	0
A2	411.6	718	925	168	5	8.4
A4	403.2	718	925	168	5	16.8
A6	394.8	718	925	168	5	25.2
A8	386.4	718	925	168	5	33.6
B2	420	718	925	168	5	8.4
B4	420	718	925	168	5	16.8
B6	420	718	925	168	5	25.2
B8	420	718	925	168	5	33.6
C1	420	710.8	925	168	5	7.2
C2	420	703.6	925	168	5	14.4
C3	420	696.4	925	168	5	21.5
C4	420	689.2	925	168	5	28.7
C5	420	682	925	168	5	35.9

2.4.2. Microstructure

The samples were degassed at 105℃ for 8 h using Quantachrome-Autosorb-IQ. Then, the pore size distribution and specific surface area of OA after pyrolysis at different temperatures were characterized by nitrogen adsorption/desorption at 77 K (BET technique). The pore size distribution was assessed through the method developed by Barrett, Joyner, and Halenda (BJH).

The morphological differences of OA before and after pyrolysis were analyzed by cold field emission scanning electron microscopy (Czech-TESCAN-MIRA4), and the differences in the microscopic morphology of concrete after the incorporation of soybean dregs biochar were characterized. Before the test, the specimen was soaked in anhydrous ethanol for 48 h and dried in vacuum drying oven at 60℃ to a constant weight. The dried specimen for SEM was gold-coated prior to the test to improve electrical conductivity.

An X-ray diffractometer (Rigaku SmartLab SE, Japan) was employed to analyze the phase composition of cement hydration products after BC incorporation. The analyses used Cu-Kα radiation with a 2θ angle ranging from 5° to 70°. The scanning speed and the resolution was 10°/min and 0.02/step, respectively.

Fourier transform infrared spectroscopy (FTIR, Spectrum Two, USA) was used to explore the types of surface functional groups after BC pyrolysis. During the test, an appropriate amount of dried biochar concrete powder and KBr powder were taken, fully ground and mixed evenly and pressed into tablets to prepare samples. The infrared spectrum measurement range was set to 500 cm^{-1}-4000 cm^{-1}. Before analyzing the test samples, the ambient atmospheric background value was collected to reduce the error. The test results were repeatedly tested three times to confirm the authenticity of the data.

3. Results

3.1. Performance characterization of BC

3.1.1. Yield

Fig. 3 illustrated the char yield of OA at different pyrolysis temperatures. The yield continuously decreased as the charring temperature increased. The char yield decreased sharply when the temperature was 300℃-500℃, followed by a gradual stabilization at temperatures above 500℃. This was due to the depolymerization of cellulose, hemicellulose, and lignin present in biomass. The decomposition temperature for cellulose and hemicellulose fell within the range of 250℃-450℃, while the decomposition of lignin was more challenging and occurred slowly

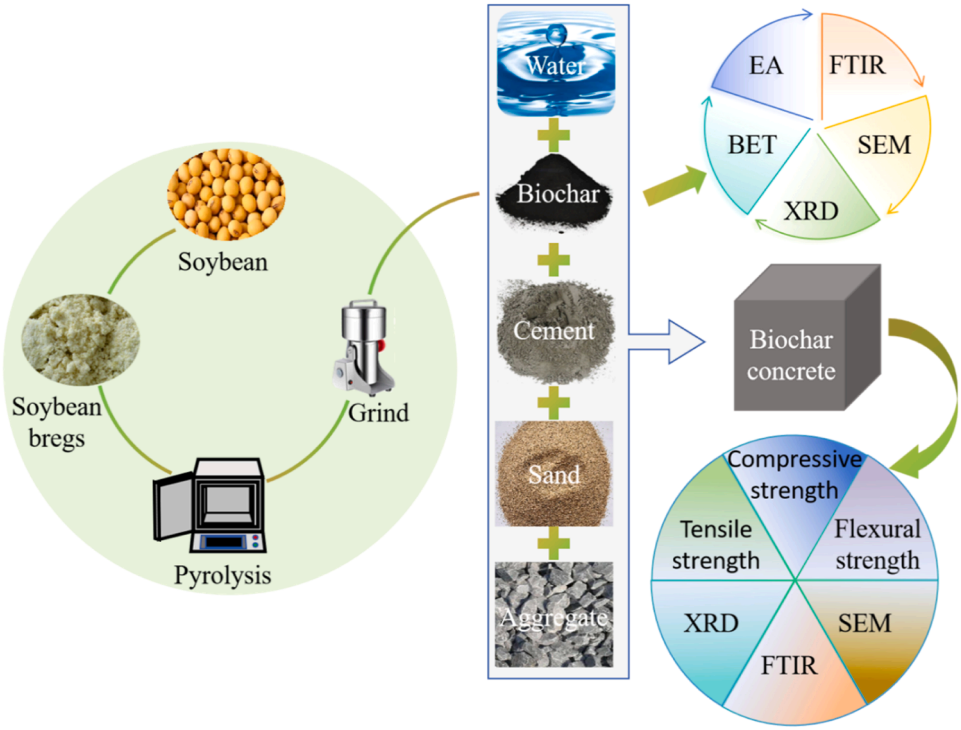

Fig. 2. Experimental process chart.

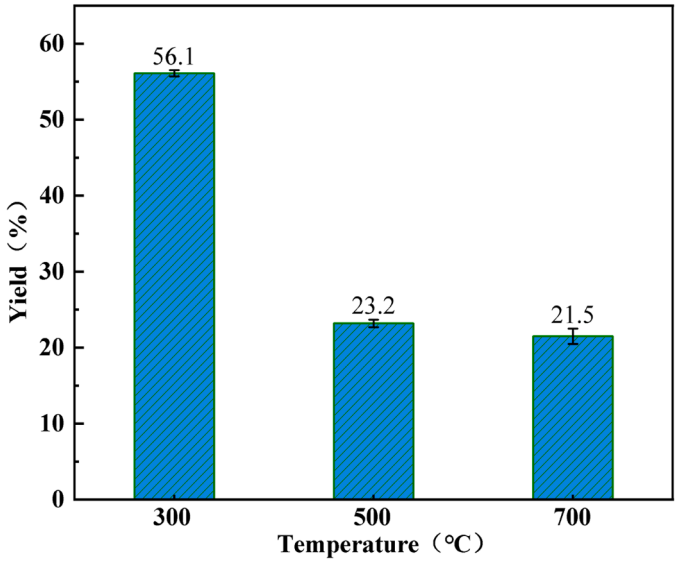

Fig. 3. Yield of OA after cracking at different temperatures.

throughout the entire pyrolysis process[18]. Consequently, the biochar yield exhibited a significant decrease starting at 300℃, with complete decomposition of cellulose occurring at 500℃-700℃ leading to a gradual stabilization of the yield.

3.1.2. BET

Specific surface area and N_2 adsorption-desorption curves were important parameters for characterizing the pore structure of biochar. The removal of organic volatiles during pyrolysis led to the formation of a favorable pore structure and a large specific surface area. Comparing the BET and N_2 adsorption-desorption isotherms of OA before and after pyrolysis, it could be observed from Table 6 and Fig. 4 that the specific surface area and N_2 adsorption-desorption of OA were relatively low.

Table 6
Specific surface area and pore structure of BC.

	OA	3BC	5BC	7BC
BET surface area (m^2/g)	3.7	4.6	5.4	14.9
Total pore volume (g/mL)	0.006	0.006	0.012	0.018
Average pore Diameter (nm)	3.6	3.6	3.6	3.6
Most probable aperture (nm)	3.1–3.3	2.7–2.9	2.7–2.9	2.7–2.9

Although 3BC and 5BC showed some improvement compared to OA, the improvement was not significant. The main reason was that the cellulose was not completely cracked during the pyrolysis of OA at 300℃-500℃, and the covalent bond was not completely broken, resulting in the volatile matter could not escape[19]. Despite the presence of some pore formations, they did not contribute to a substantial pore structure, resulting in a low specific surface area and insignificant N_2 adsorption enhancement. However at 500℃-700℃, cellulose, hemicellulose, and lignin in OA were completely decomposed. The volatile gas produced during pyrolysis escapes, so that the micropores in biochar developed well and the pore volume increased, thus forming a rich pore structure. As a result, the specific surface area and N_2 adsorption capacity increased significantly. At 700℃, the volatile fraction was completely released, the pore structure was essentially formed, and the N_2 adsorption reached its maximum value. This could be demonstrated by the BJH aperture distribution in Fig. 4 and the most available aperture distribution in Fig. 5. When compared to OA, the pore size of 3BC and 5BC did not decrease significantly after pyrolysis, but the pore volume increased, indicating the generation of new mesopores. The new and existing mesopores in the range of 5–20 nm of 7BC gradually transformed into micropores after exposure to high temperatures of 700 ℃, and the sharp increased in pore volume also confirmed this observation.

3.1.3. XRD

The XRD patterns of OA after pyrolysis at different temperatures are displayed in Fig. 6. At temperatures below 300℃, a broad hump appeared at around $2\theta = 19.57°$[20,21], which corresponds to the

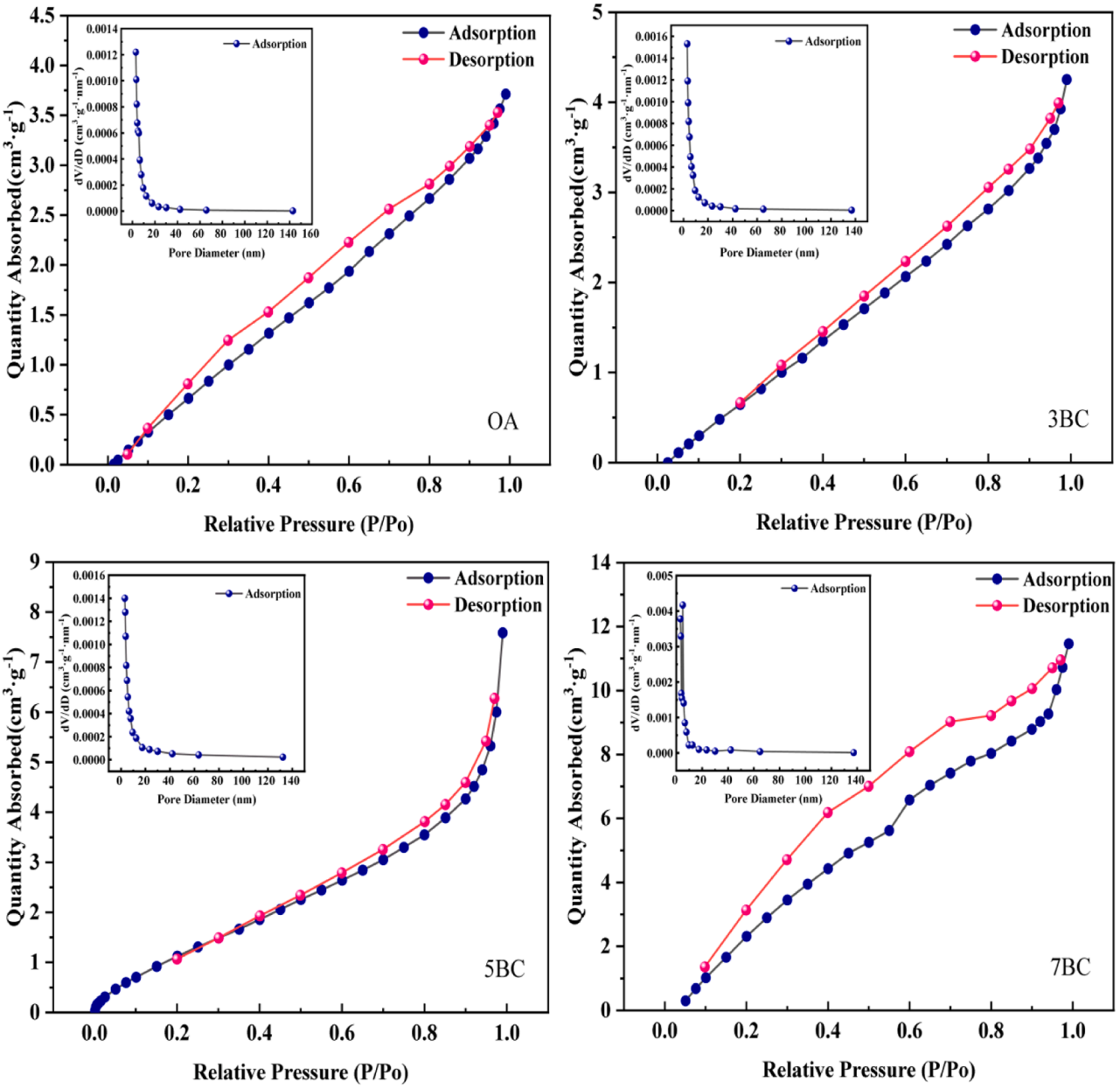

Fig. 4. N_2 adsorption curve of OA after cracking at different temperatures.

diffraction peak of hemicellulose[22]. The charring of hemicellulose at high temperatures led to a weakening of its diffraction peaks, and the cellulose gradually transformed into microcrystalline carbon fibers after charring[23]. Another hump appeared near 2θ= 24.84°[24,25], indicating the presence of broad diffraction peaks of graphite microcrystals (002)[26]. The shift of the diffraction peak to a larger angle could be attributed to the increase in carbonization temperature, which further promoted the carbonization of biochar and facilitated the growth of graphite microcrystals. The cellulose in the biochar gradually transformed into a graphitic structure, and the disordered carbon structure continuously transformed into highly ordered carbon compounds with increased crystallinity, resulting in the formation of a structurally stable aromatic structure.

3.1.4. FTIR

The functional group types of OA before and after pyrolysis were investigated using FTIR, and the results were shown in Fig. 7. Both before and after pyrolysis, OA exhibited broad peaks at 3419 cm^{-1}, which was mainly attributed to the stretching vibration of hydroxyl (O-H) in the alcohol and phenol structures associated with intermolecular hydrogen bonds. After high-temperature pyrolysis, the biochar gradually underwent aromatization, resulting in increased hydrophobicity. This led to a decrease in the peak of the O-H absorption in the BC after high-temperature pyrolysis of OA. The peak near 2925 cm^{-1} corresponded to the stretching vibration of the C-H bond. The peaks of BC were weaker after pyrolysis at different temperatures compared to OA. This could be attributed to the fact that the increase in charring temperature induced the depolymerization and breakage of the alkyl chains in the biochar, leading to the stabilization of the biochar[27]. The absorption peak at 1745 cm^{-1} reflected the stretching vibration of the carbonyl (C═O) bond in the aldehyde and ketone structures[28]. At higher pyrolysis temperatures, due to the decarboxylation reaction, 7BC showed a weaker peak at 1745 cm^{-1}. The absorption peak near 1591 cm^{-1} predominantly represented the stretching vibration of the alkene (C═C) bond. As the temperature increased, the peak of C═O gradually decreases, while the peak of C═C increases, indicating that

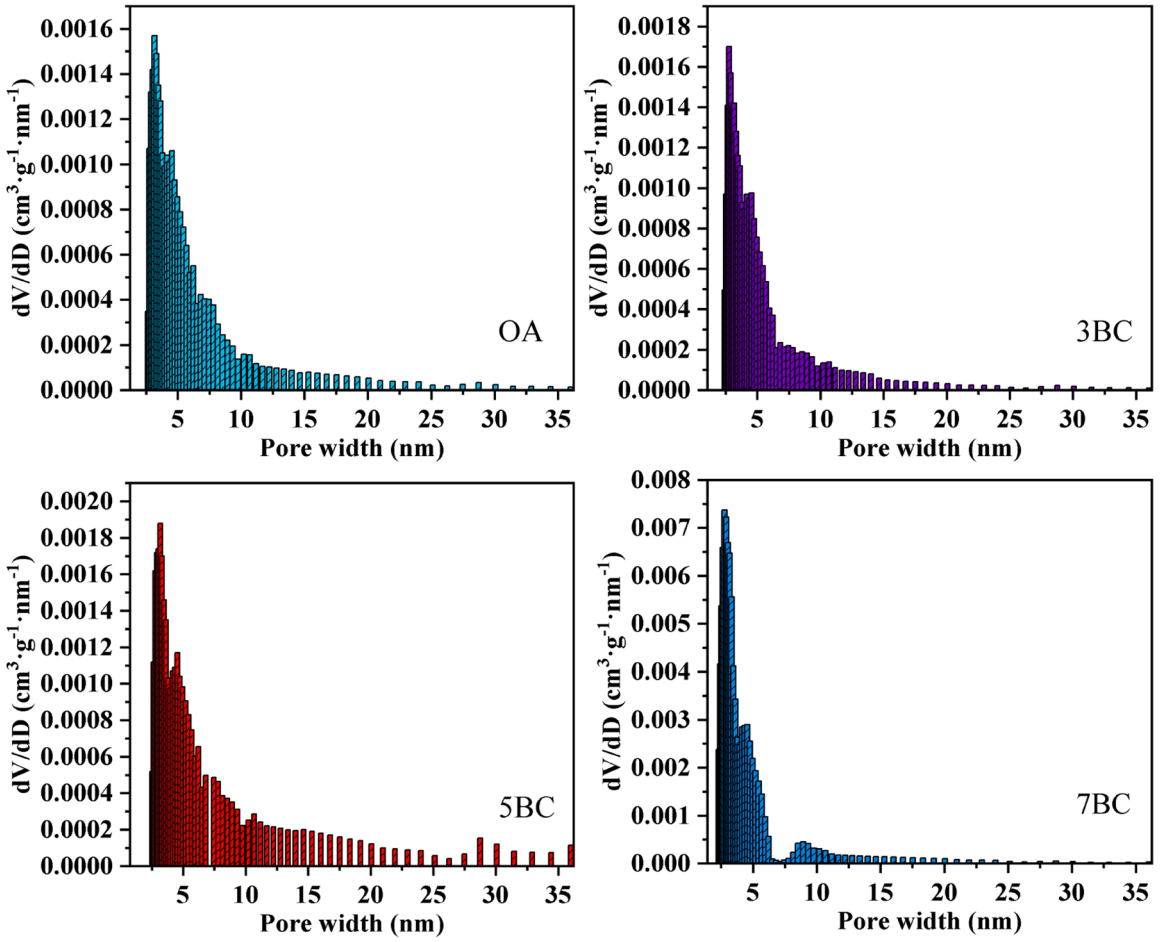

Fig. 5. Distribution on most probable aperture of OA after Pyrolysis.

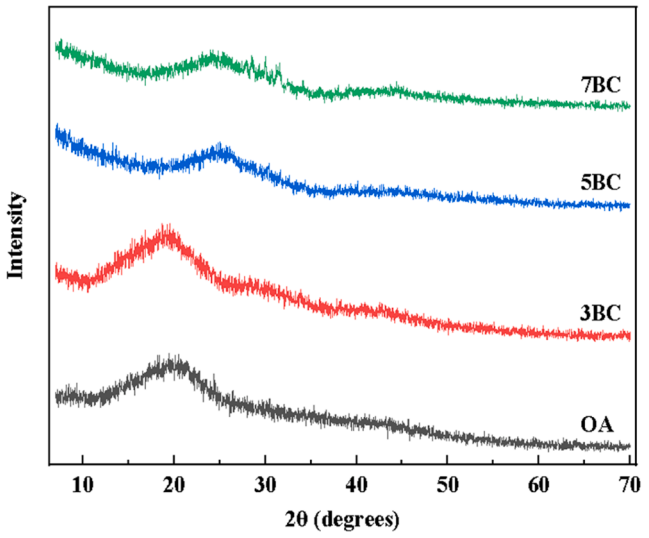

Fig. 6. XRD analysis of OA pyrolysis at different temperatures.

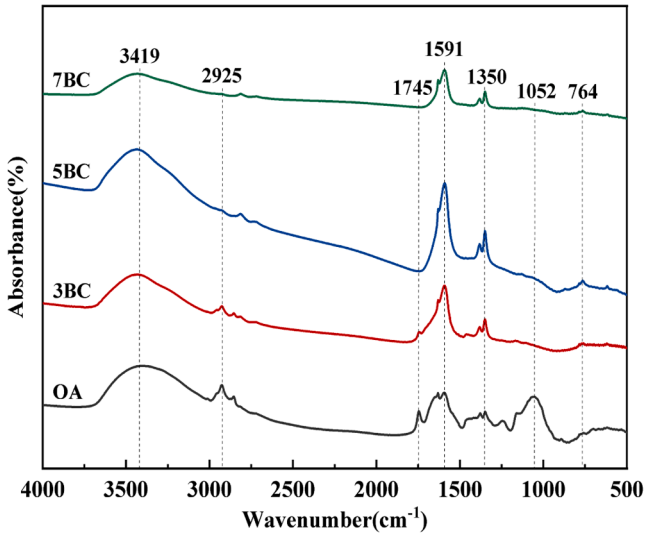

Fig. 7. FTIR analysis of OA pyrolysis at different temperatures.

high temperature promoted the aromatization degree of biochar. The absorption peak at around 1350 cm^{-1} indicated the presence of N = O in BC, which originated from amino acids and fatty substances in OA [29]. The extremely strong vibration peak at 1052 cm^{-1} corresponded to the C-O-C stretching vibrations in cellulose and hemicellulose. The weak peak fluctuation at 1052 cm^{-1} in BC was due to the complete decomposition of cellulose at higher pyrolysis temperature, which further confirmed a high cellulose content in OA. Meanwhile, the characteristic peak at 764 cm^{-1} represented the oriented bending vibration of the aromatic hydrocarbon C-H bond, providing evidence for the highly aromatic nature of BC. These changes in functional groups indicated that high-temperature pyrolysis of OA was an aromatization

process, which promoted the formation of aromatic groups and increased the structural stability.

3.1.5. SEM

The microstructure of OA before and after pyrolysis was characterized by SEM, as shown in Fig. 8. OA exhibited a smooth and dense surface with irregular and folded structures, and no visible pore structure. The morphology of 3BC was similar to that of OA, exhibiting a complete and smooth surface without any obvious pore structure. This indicated that the cellulose in OA was not cracked at 300℃, and the internal structure remained largely unchanged. Although some pores were observed on the surface of 5BC, they were not fully developed, indicating that the cellulose in OA was still not completely decomposed. The surface morphology of 7BC underwent a significant change, with the appearance of numerous pores. Compared to 5BC, the pore structure in 7BC was more compact and uniform, which corresponded to its higher specific surface area and smaller pore size distribution. The different structures observed in OA after pyrolysis at different temperatures could be attributed to the release of organic matter and volatile substances from OA at high temperatures. The escape of volatiles destroyed the original structure of OA and promoted the formation of pore structure. The biochar prepared at 700℃ exhibited a greater number of uniform pores compared to those prepared at 300℃ and 500℃. This could be attributed to the more complete cracking of volatile compounds in the raw materials as the pyrolysis temperature increased to a certain extent.

3.2. Properties of biochar concrete

3.2.1. Workability

The slump in each group of concrete was shown in Fig. 9. The results showed that the slump of concrete was lower than that of the control group regardless of the way of adding biochar into concrete. And the three ways of addition showed a consistent pattern that the slump of concrete gradually decreased with the increase of biochar content. The decreased in slump was relatively gradual at a dosage of 2 %, but it decreased significantly with a dosage exceeding 2 %. BC possessed a large specific surface area and a porous structure, which enhanced its ability to compete with cement for free water during the mixing process. Additionally, the carbon structure of BC contributed to its favorable cation exchange capacity[30]. During concrete mixing, some of the free water could be rapidly adsorbed through hydrogen bonding, and the reduction of available free water increases the friction between the components of the mixture. As the amount of BC increased, water

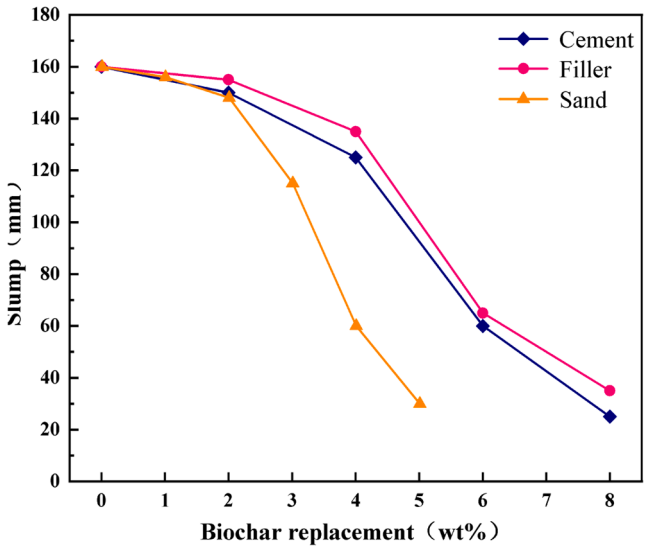

Fig. 9. The slump of BC concrete.

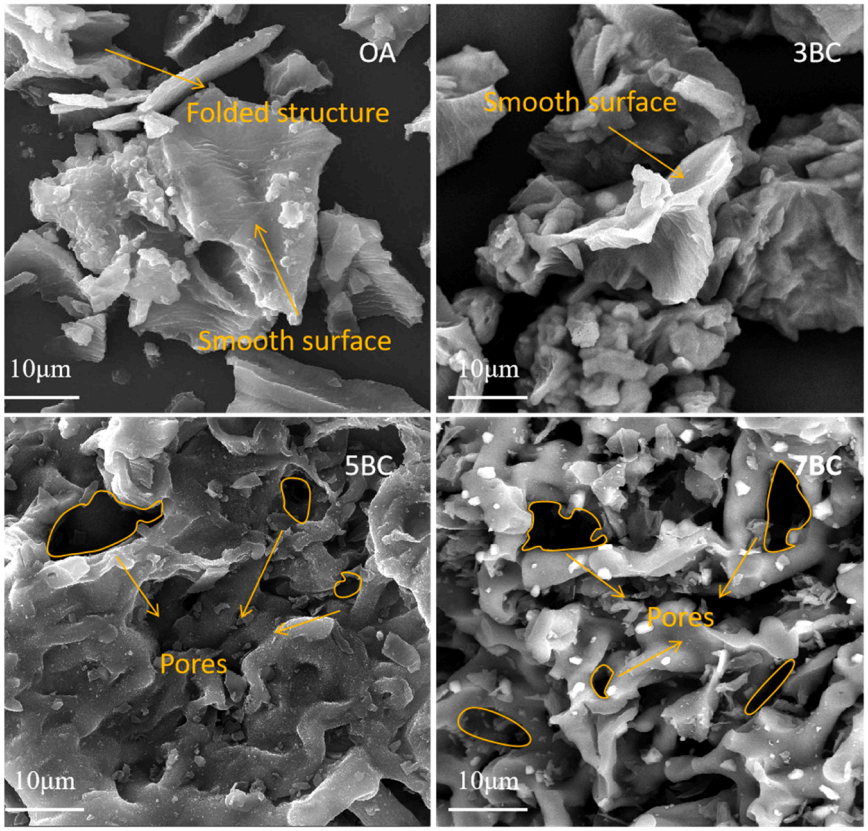

Fig. 8. Scanning electron microscope image of OA before and after pyrolysis.

absorption also increased, along with the irregular shape of BC particles, which did not ensure effective bead-carrying action[31]. Consequently, this led to a sharp declined in the workability of the concrete.

3.2.2. Compressive strength

The compressive strength of BC concrete after 28 d of curing was indicated in Fig. 10. The compressive strength of each group of concrete increased with the enhancement of BC content and then decreased. In Group A, when cement was replaced with BC at a dosage of 2 %, the strength of the sample increased by 7.19 % compared to the control group. However, at a substitution rate of 4 %, the compressive strength of concrete was similar to that of the control group. As the dosage continued to increase, the strength started to decrease. At dosage of 6 %, the strength was still in line with the strength requirements of C40 concrete, although there was a loss of 6.78 %. When the dosage increased to 8 %, the strength of BC concrete was lower than that of C40, with a loss of 16.43 %. The strength trend in Group B, where BC acted as filler, was similar to that of Group A. The best compressive strength at 2 % admixture was 50.83 MPa, which was 9.86 % higher than that of the control group. However, there was a significant decrease trend in strength as the content continued to increase. In Group C, where sand was replaced with BC, the compressive strength of the concrete was better than that of Groups A and B. Among them, at a substitution rate of 3 %, the compressive strength reached 51.97 MPa, with an enhancement rate of 12.32 %.

When BC was added to concrete as a substitute for cement, there was not a significant improvement in compressive strength. This could be attributed to the relatively low silica content of BC compared to other types of biochars, which could not improve the effective volcanic ash effect. However, the addition of BC at low doses did lead to an increase in strength due to its filling effect. Furthermore, as the dosage of BC increased, the cement content decreased, leading to a decrease in the yield of hydration products (C-S-H). C-S-H was crucial for the development of concrete strength, and the decrease in its content reduced the compressive strength of the concrete. When BC was used as a filler or as a replacement for sand in concrete, it demonstrated a relatively remarkable increase in compressive strength compared to its use as a cement substitute. Gupta[32]also utilized wood waste biochar as a filler and found that the compressive strength showed the most significant improvement at a content level of 2 %.

The increase in strength might be attributed to the finer-sized biochar, which effectively filled the pores within the paste compared to cement and sand particles. Additionally, biochar served as a nucleation matrix for hydration products such as C-S-H in the cement matrix, thereby enhancing the micropore structure of concrete. Furthermore, the high carbon content in BC made it have a good water retention capacity, promoting hydration during the later stages of concrete curing. BC absorbed some of the water during the initial mixing of the concrete, resulting in a localized reduction in the water-cement ratio, which decreased the number of internal capillary pores and promoted the densification of the paste within the concrete[32]. As the concrete hardens during the curing process, the hydration of the cement consumed the water in the capillaries, leading to a decrease in internal relative humidity. This reduction resulted in a pressure difference between cement and BC, which caused BC to desorb the water absorbed during the early curing process and promoted the further hydration of the unhydrated clinker inside the paste[15]. Additionally, the smaller particle size of BC reduced the spacing coefficient, which meant that the water released from the biochar pores only needed to move a shorter distance within the matrix to provide effective curing[17], making the concrete mechanically stronger. When BC was overdosed, the agglomeration effect occurred internally, forming weak zones due to its rough and irregular surface[33], both of which were important for the bonding of biochar to the cement paste. The increase of BC content made it absorb too much water in the process of concrete mixing, which weakened the hydration of cement and led to a decrease in compressive strength.

3.2.3. Tensile and flexural strength

The splitting tensile and flexural strength of concrete with different admixtures of BC were indicated in Fig. 11 and Fig. 12. Similar to the trend observed in compressive strength, BC exhibited the greatest enhancement in the tensile and flexural strength of concrete at lower content levels. When BC replaced 2 % of the cement, the tensile and flexural strength of biochar concrete enhanced by 7.46 % and 4.41 %, respectively. When the same dosage of BC was used as a filler, the strength enhancement rates were 12.54 % and 4.85 %, respectively. When BC replaced 3 % of the sand, the tensile and flexural strength enhancement rates was as high as 16.42 % and 8.24 %, respectively. The strength enhancement after cement replacement was relatively low for all three different BC contents. Mixing BC with concrete as a filler and replacing sand yielded better enhancement of its mechanical properties, but the more significant performance improvement was achieved when BC was used as a replacement for sand. When BC was used as filler, the sand ratio increased with the increase of BC dosage. However, when BC

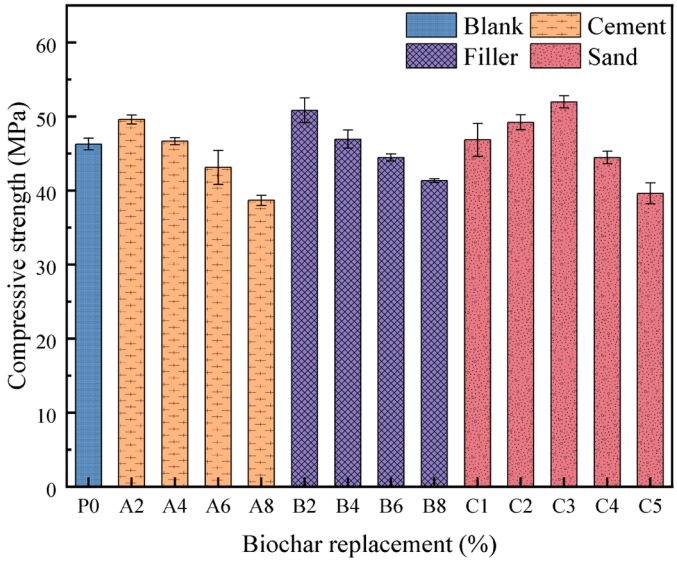

Fig. 10. Compressive strength of BC concrete.

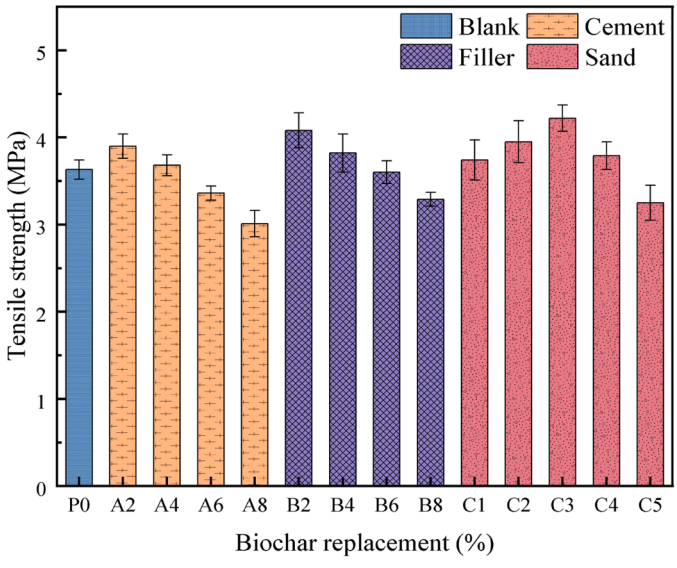

Fig. 11. Tensile strength of BC concrete.

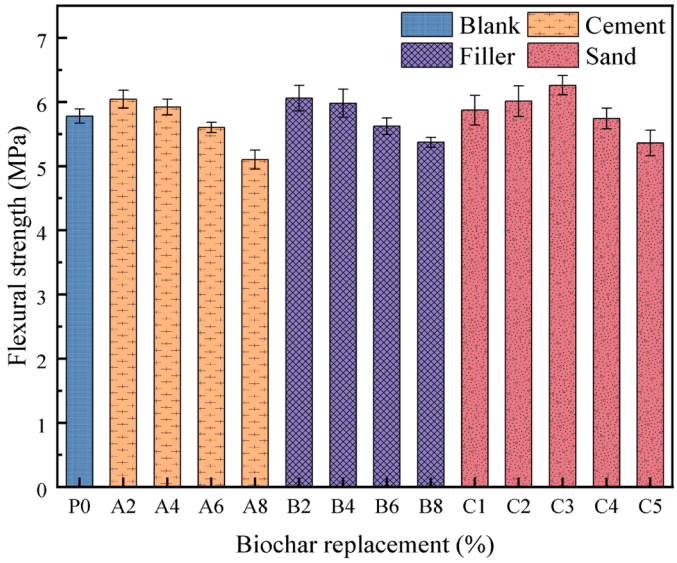

Fig. 12. Flexural strength of BC concrete.

replaced sand, the sand rate was consistent with the blank group. A reasonable sand rate enabled BC to exert a favorable filling effect, thereby influencing the improvement of concrete performance. Praneeth et al. [34]reported that substituting 20 % poultry bedding biochar for 10 %-40 % of the sand resulted in a 26 % increase in flexural strength compared to control mortar.

Compared to the compressive and tensile strength, the increment in flexural strength of concrete was indistinctive, even with a low admixture. There was no significant decrease in flexural strength, even with a high dosage, when BC was incorporated in any manner, compared to the control group. The loss in flexural strength for A8, B8, and C5 was 11.76 %, 7.06 %, and 7.21 %, respectively, while the compressive and tensile strength decreased by 16.43 %, 10.68 %, 14.37 %, and 17.16 %, 9.4 %, 10.47 %, respectively. There was no significant negative effect of BC on flexural strength as compared to compressive and tensile strength, which might be due to the weaker modulus of elasticity of BC particles [35]. Akhtar[10]showed that the augmentation in flexural strength could be attributed to the flexibility provided by the biochar in the cemented composites, which acted as a link between the cement and the biochar particles to avoid chances of early fracture. The incorporation of biochar induced a diminution in pore size and the number of macropores in the matrix, leading to an increase in flexural strength.

The increase in tensile and flexural strength might also be related to the refinement of the interfacial transition zone (ITZ). The incorporation of a small amount of BC reinforced the transition region between cementitious materials and aggregates[36] and reduced the large amount of calcium hydroxide crystals and impurities, resulting in the densification of the microstructure. The smaller amount of BC incorporated into the concrete could impede the propagation of cracks by acting as a barrier to the development of micro-cracks. So that it could not be directly through and offset from the perimeter, which could be split into a number of fine cracks to form zigzag fracture cracks. At this time, the concrete was capable of withstanding higher energy during the splitting process, thereby reducing brittleness enhancing resistance to cracking. As shown in Fig. 13, ordinary concrete directly broke into two halves after being subjected to load, and the fracture cracks directly penetrated the specimen. Under the action of load, due to the existence of soybean dregs biochar, the fracture crack propagation was hindered, and the soybean dregs biochar concrete was divided into two fine cracks.

The SEM revealed that a small amount of biochar incorporated into the cement paste was tightly attached, with no visible gap. Under tensile loading, ordinary concrete usually split into two pieces at the boundary gap between the sand particles and the cement stone[37]. In biochar concrete, the area where the biochar was closely connected to the cement stone was smooth and strengthened the boundary of concrete against cracking[38,39]. The microcracks neither extended into the region nor bridged to other cracks around the biochar particles, and the microcracks did not pass through the biochar particles. Therefore, moderate amount of biochar increased the split tensile and flexural strength of the concrete. However, when a large amount of porous biochar was incorporated, it caused internal agglomeration, which reduced the crack hindering effect of the biochar particles. This weakened the matrix of the concrete and created voids in the tensile plane, reducing the effective cross-sectional load-bearing area[35]. As a result, the force required for the expansion of internal fissures decreased, leading to a diminution in the strength of concrete.

The tension-compression ratio of concrete was an index to survey the brittleness of concrete. A higher tension-compression ratio showed less brittleness and more plasticity in the concrete[40]. The flexural-compression ratio was a measure of the tenacity of concrete. A larger ratio indicated that the concrete was more ductile and more resistant to cracking[41]. Fig. 14 demonstrated that regardless of the way BC was incorporated into the concrete, the tensile-compression ratio was improved compared to the control group, with a maximum enhancement rate of 8.7 %. The addition of BC reduced the brittleness of concrete and improved its plastic properties. In contrast, the flexural-compression ratio differed from that of the concrete with optimal mechanical properties, as it reduced compared to the control group, resulting in reduced toughness. The toughness of the concrete improved after 4 % dosage and gradually increased with higher dosages, with the maximum enhancement reaching up to 8.4 %.

3.3. *Microscopic analysis of biochar concrete*

3.3.1. *XRD*

Fig. 15 demonstrated the XRD patterns of BC concrete at 28 d. The XRD patterns indicated that the addition of biochar to the concrete did not introduce any new phases and did not cause a shift in the peaks. The

Fig. 13. Crack expansion in BC concrete.

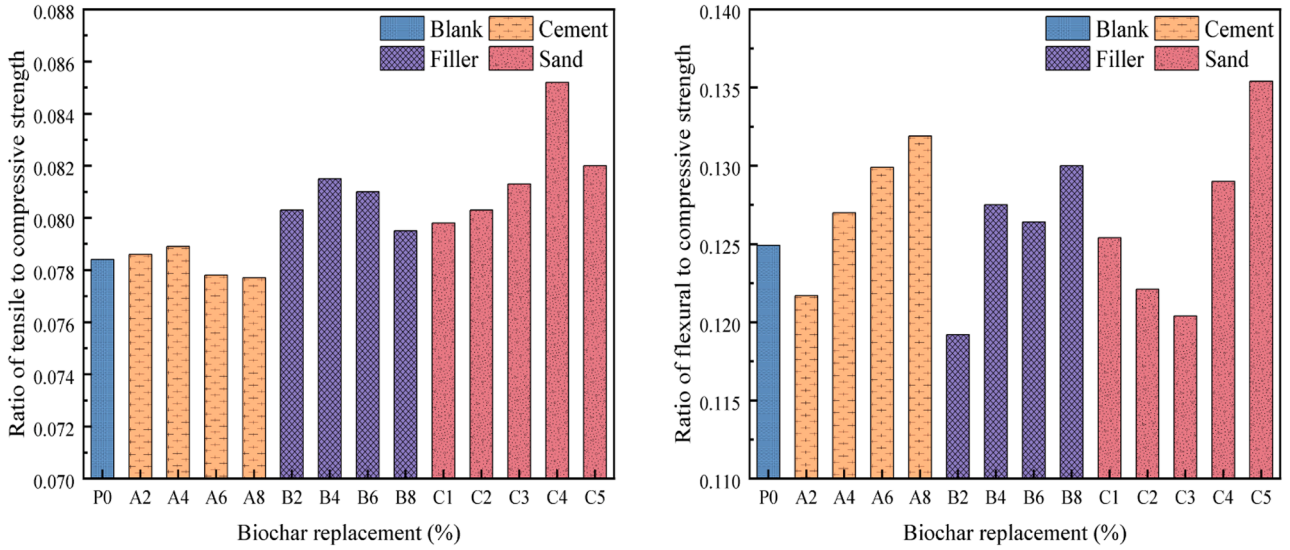

Fig. 14. Tension-compression and flexural-compression ratio of BC concrete.

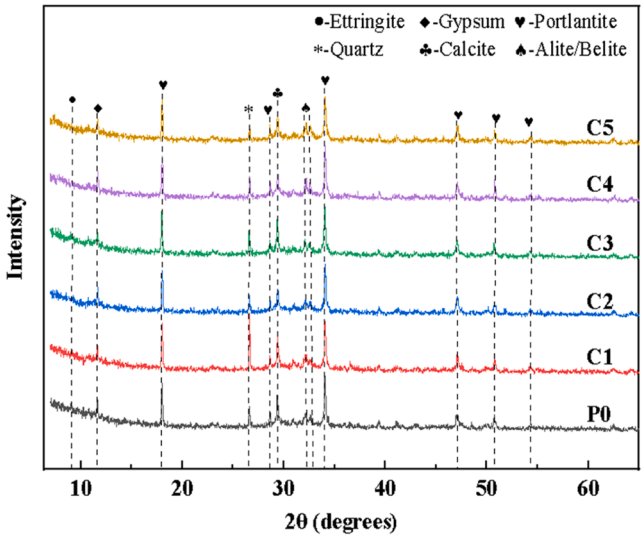

Fig. 15. XRD patterns of BC concrete.

various diffraction peaks indicated the presence of ettringite ($3CaO{\cdot}Al_2O_3{\cdot}CaSO_4{\cdot}32\ H_2O$, PDF-2 no. 41–1451), quartz (SiO_2, PDF-2 no. 46–1045), portlandite ($Ca(OH)_2$, PDF-2 no. 44–1481), calcite ($CaCO_3$, PDF-2 no. 24–0027), calcium silicate ($3CaO{\cdot}SiO_2/2CaO{\cdot}SiO_2$, PDF-2 no. 49–0442/29–0369), and gypsum ($CaSO_4{\cdot}2\ H_2O$, PDF-2 no. 33–0311), suggesting the presence of both hydration products and some unhydrated components in the slurry[42]. The hydrated calcium silicate was poorly crystallized and not marked in the figure. The weak peak at 2θ of 9.1° showed the presence of ettringite (AFt). The peak of AFt reached the maximum in C3, and with the increase of biochar content, the peak gradually weakened. The peak at 26.6° appeared in all the diffractograms, and the SiO_2 diffraction peaks increased slightly after the incorporation of biochar, probably due to the BC itself containing traces of SiO_2. Prominent peaks at 2θ values of 18.0°, 28.6°, 34.1°, 47.2°, and 50.8° indicated the existence of $Ca(OH)_2$[43]. Compared to the control group, the peak value of $Ca(OH)_2$ increased slightly when BC was doped with 1 %, indicating that BC could promote hydration. However, the peak value of $Ca(OH)_2$ gradually decreased with the increase of BC doping, which may be that the doping with biochar promoted the delayed hydration of cement[44,45]. The peak value of C_3S/C_2S at 32° was weakened after adding biochar, which also reflected that the addition of biochar promoted the hydration of cement. The peak at 2θ values of 29.37° indicated the existence of $CaCO_3$. Biochar could provide a rich place for the dissolution of CO_2 to promote carbonization [15,46]. Therefore, the peak value of $CaCO_3$ in C1 increased slightly.

3.3.2. FTIR

Fig. 16 shows the infrared spectra of concrete with different dosages of biochar after 28 d of curing. The absorption peak at 3643 cm^{-1} was the peak of stretching vibration of -OH and O-H bonds in $Ca(OH)_2$ and H_2O. The occurrence of a weak peak at 2926 cm^{-1} demonstrated the existence of C-H, and the v_2 bending vibration of the hydroxyl group resulted in the weak peak at 1593 cm^{-1}. The absorption peak at 1417 cm^{-1} was considered to be the peak of flexural oscillation of CO_3^{2-}, confirming the presence of paste with calcium carbonate[47], and its peak intensity was associated with the carbonation reaction. The small peak at 1110 cm^{-1} corresponded to the presence of C═O bonds. Meanwhile, the peaks at 965 cm^{-1} and 875 cm^{-1} were absorption peaks caused by extensional vibrations of C-O and Si-O bonds, which also indicated the presence of C-S-H[10]. Overall, the content of $Ca(OH)_2$ decreased relatively with the addition of biochar, while the content of

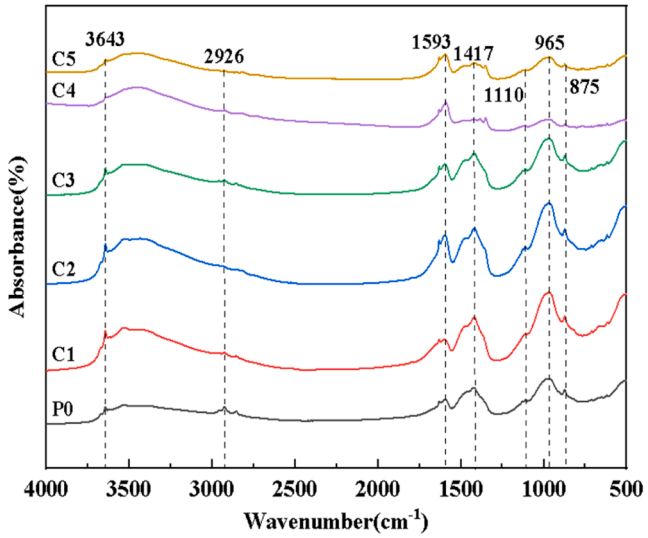

Fig. 16. FTIR patterns of BC concrete.

C-S-H increased.

On the whole, the band at 965 cm^{-1} was associated with C-S-H. The highest strength at 1 %-3 % biochar doping indicated that the incorporation of biochar in the cement composites formed a wealth of C-S-H [48]. The peak area at 1417 cm^{-1} increased with 1 %-3 % biochar substitution, indicating an increase in the content of calcium carbonate. The formation of calcium carbonate originated from the carbonation reaction of $Ca(OH)_2$ with CO_2 in the pore water[49]. This showed that biochar not only served as a filler to fill in the cement paste, but its porous structure also stored water and provided abundant sites for CO_2 dissolution, thereby promoting carbonation. The weakening of the bands at 1417 cm^{-1} and 965 cm^{-1} for dosages above 4 % suggested a reduction in the content of hydrated calcium silicate, leading to a weakening of the hydration reaction and a subsequent decrease in its mechanical properties.

3.3.3. SEM

To better understand the impact of BC on the microstructure of concrete, the micro-morphology was observed using SEM. Fig. 17 revealed the SEM images of concrete after 28 d of curing under three different methods of BC incorporation. The surface morphology of concrete after adding lower BC showed a uniform and dense structure. The irregular shape of the BC particles could be used as a filler to fill the fine pores within the concrete microstructure, resulting in a dense paste matrix with low porosity and relatively small pore size[32]. Most of the internal hydration products were dominated by needle-and-rod AFt and flocculated C-S-H, with a relatively small amount of layered $Ca(OH)_2$. The porous structure of pyrolyzed BC released the water absorbed during paste mixing during the post-curing process of concrete, and the consumption of $Ca(OH)_2$ prompted further hydration reaction[45]. With the increased of BC content, many pores were formed on the surface of the slurry, rather than a dense network structure. The hydration products were mainly dominated by layered $Ca(OH)_2$, with relatively little AFt and C-S-H. The high dosage of BC absorbed too much water during the mixing process, which hindered cement hydration to some extent.

While the C-S-H were mainly used to bond the other components to form a dense system and provide the late strength of the concrete[50]. The decrease in the content of C-S-H led to an increase in the number of pores and a decrease in the bonding, densification, and strength between the crystals. This was most evident in A6(a) and B6(a), where distinct pores were observed on the surface. In B6(b), some BC remained in the slurry due to overmixing. The interface was loose and porous, and the presence of excess pores resulted in a reduction in concrete strength. The surface of C5(a) had fewer pores compared to it, which explained the

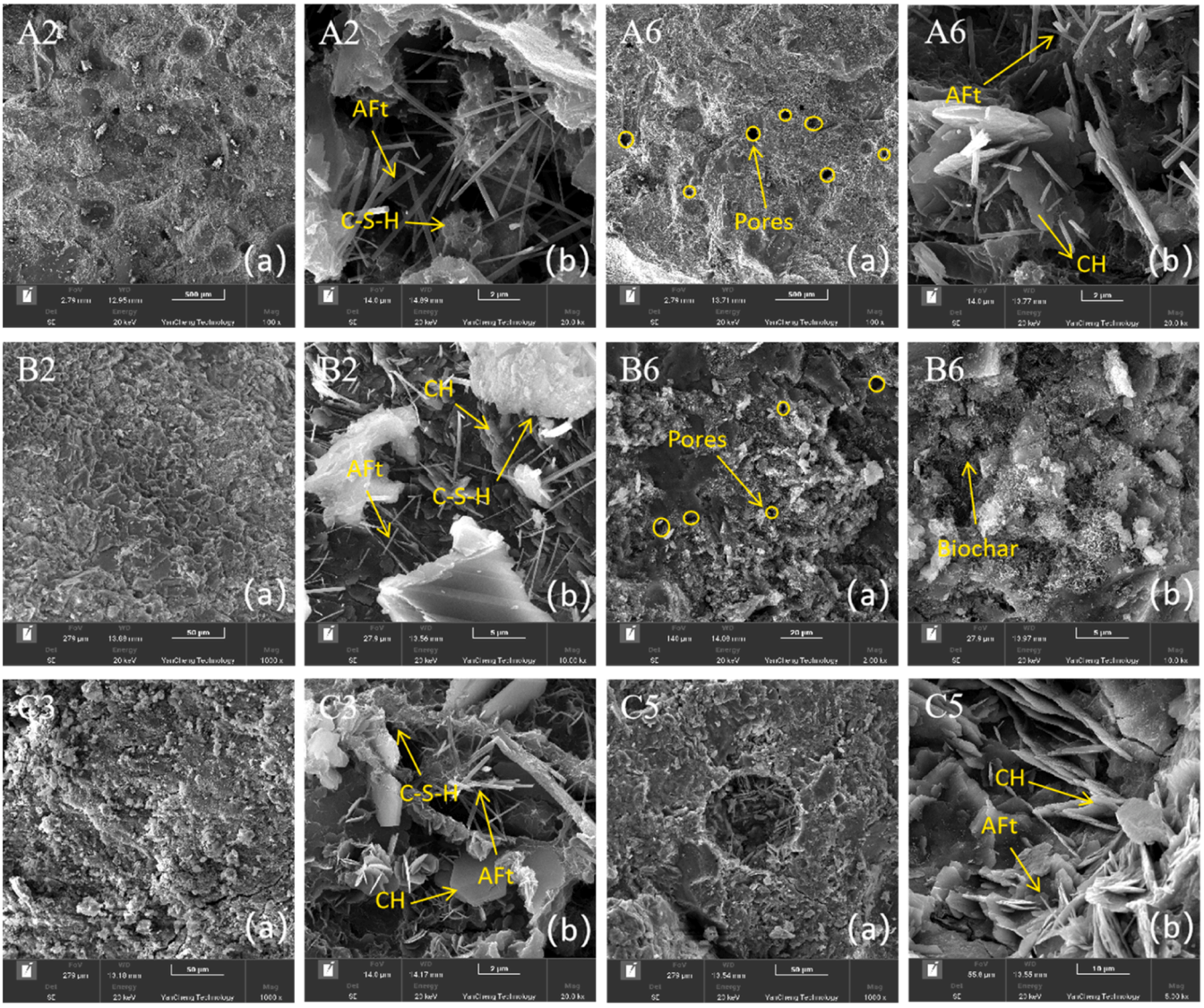

Fig. 17. SEM of BC concrete at low(a) and high(b) magnifications.

higher strength of Group C compared to Groups A and B. This indicated that BC as a replacement of sand had better performance enhancement for concrete.

4. Conclusion and recommendation

In this study, soybean dregs biochar was incorporated into concrete using different methods and substitution amounts to determine its optimal incorporation in concrete. The main conclusions of the study were summarized as follows:

(1) The mesopores inside the soybean dregs gradually transformed into micropores as the temperature increased. After high-temperature pyrolysis at 700℃, soybean dregs biochar had the largest specific surface area and the most abundant pore structure.
(2) The favorable micropores structure of soybean dregs biochar led to a decrease in slump as the substitution rate increased, regardless of the method of incorporation into the concrete.
(3) The mechanical properties of concrete, especially the compressive and tensile strength, were improved by replacing sand with soybean dregs biochar due to its favorable filling effect. The optimal replacement rate was found to be no more than 4 %.
(4) The incorporation of a small amount of soybean dregs biochar increased the content of hydrated calcium silicate within the concrete. The finer particle size effectively filled the pores in the concrete, resulting in a denser structure and enhancing the strength of the concrete.

In future research, the effects of other treatment processes on the properties of soybean dregs biochar could be further explored. Additionally, the durability, functionality, and ecological benefits of soybean dregs biochar concrete should be studied in depth.

CRediT authorship contribution statement

Zheng Chen: Writing – review & editing, Funding acquisition, Conceptualization. **Jie Shao:** Investigation. **Shujian Luo:** Investigation. **Deliang Yu:** Methodology. **Shujie Liu:** Writing – original draft, Methodology, Investigation, Data curation.

Declaration of Competing Interest

The authors declare that they have no known competing financial interests or personal relationships that could have appeared to influence the work reported in this paper.

Acknowledgements

This research was supported by the Research Project of the Shaanxi Provincial Natural Science Foundation Project (2022JM-293) and the Central University Foundation Project (CHD, 300102213511).

Data Availability

Data will be made available on request.

References

[1] Z.S. Zhang, S.P. Ye, Q. Li, et al., Handling and processing of soybean dregs, Food Sci. 25 (10) (2004) 400–406.
[2] W.Y. Mo, Y.B. Man, M.H. Wong, Use of food waste, fish waste and food processing waste for China's aquaculture industry: needs and challenge, Sci. Total Environ. 613-614 (2018) 635–643.
[3] L.J. Leng, H.J. Huang, H. Li, et al., Biochar stability assessment methods: a review, Sci. Total Environ. 647 (2019) 210–222.
[4] S.M. Shaheen, A. El-Naggar, J. Wang, et al., Biochar as an (Im)mobilizing agent for the potentially toxic elements in contaminated soils, Biochar Biomass. Waste (2019) 255–274.
[5] J. Li, Y.T. Liu, X.Y. Ren, et al., Soybean residue based biochar prepared by ball milling assisted alkali activation to activate peroxydisulfate for the degradation of tetracycline, J. Colloid Interface Sci. 599 (2021) 631–641.
[6] D.X. Shan, Z.Y. Shao, X. Liu, et al., Efficient adsorption of three dyes by soybean residue (okara) biochar in an aqueous solution, Desalin. Water Treat. 266 (2022) 212–225.
[7] B. Wang, Y.B. Zhai, T.F. Wang, et al., Fabrication of bean dreg-derived carbon with high adsorption for methylene blue: effect of hydrothermal pretreatment and pyrolysis process, Bioresour. Technol. 274 (2019) 525–532.
[8] S. Cai, Q. Zhang, Z.Q. Wang, et al., Pyrrolic N-rich biochar without exogenous nitrogen doping as a functional material for bisphenol A removal: performance and mechanism, Appl. Catal. B: Environ. 291 (2021) 1–10.
[9] C. Meyer, The greening of the concrete industry, Cem. Concr. Compos. 31 (8) (2009) 601–605.
[10] A. Akhtar, A.K. Sarmah, Novel biochar-concrete composites: manufacturing, characterization and evaluation of the mechanical properties, Sci. Total Environ. 616-617 (2018) 408–416.
[11] Z. Chen, D.L. Yu, Z.G. Feng, Aging resistance and microcharacteristics of asphalt modified by biochar from spent coffee grounds, J. Mater. Civ. Eng. 36 (9) (2024) 05024008.
[12] J. Lau, G. Biscontin, D. Berti, Effects of biochar on cement-stabilised peat soil, Proc. Inst. Civ. Eng. - Ground Improv. 176 (2) (2023) 76–87.
[13] D. Suarez-Riera, L. Restuccia, G.A. Ferro, The use of biochar to reduce the carbon footprint of cement-based materials, Procedia Struct. Integr. 26 (2020) 199–210.
[14] D. Berti, G. Biscontin, J. Lau, Effect of biochar filler on the hydration products and microstructure in portland cement–stabilized peat, J. Mater. Civ. Eng. 33 (10) (2021) 04021263.
[15] L. Wang, L. Chen, D.C.W. Tsang, et al., Biochar as green additives in cement-based composites with carbon dioxide curing, J. Clean. Prod. 258 (2020).
[16] A. Sirico, P. Bernardi, C. Sciancalepore, et al., Biochar from wood waste as additive for structural concrete, Constr. Build. Mater. 303 (2021).
[17] J. Castro, L. Keiser, M. Golias, et al., Absorption and desorption properties of fine lightweight aggregate for application to internally cured concrete mixtures, Cem. Concr. Compos. 33 (10) (2011) 1001–1008.
[18] H. Yang, R. Yan, H. Chen, et al., Characteristics of hemicellulose, cellulose and lignin pyrolysis, Fuel 86 (12-13) (2007) 1781–1788.
[19] C. Bouchelta, M.S. Medjram, M. Zoubida, et al., Effects of pyrolysis conditions on the porous structure development of date pits activated carbon, J. Anal. Appl. Pyrolysis 94 (2012) 215–222.
[20] M. Wada, R. Hori, U.-J. Kim, et al., X-ray diffraction study on the thermal expansion behavior of cellulose Iβ and its high-temperature phase, Polym. Degrad. Stab. 95 (8) (2010) 1330–1334.
[21] A. Shaaban, S.-M. Se, N.M.M. Mitan, et al., Characterization of biochar derived from rubber wood sawdust through slow pyrolysis on surface porosities and functional groups, Procedia Eng. 68 (2013) 365–371.
[22] Z.-H. Jiang, Z. Yang, C.-L. So, et al., Rapid prediction of wood crystallinity in Pinus elliotii plantation wood by near-infrared spectroscopy, J. Wood Sci. 53 (5) (2007) 449–453.
[23] Q.F. Zhen, Z.M. Wang, B.G. Chen, Structural characterization of prepared biochar and XRD spectroscopic analysis of carbonization mechanism, Spectrosc. Spectr. Anal. 36 (10) (2016) 3355–3359.
[24] B. Biswas, P. Balla, B.B. Krishna, et al., Physiochemical characteristics of bio-char derived from pyrolysis of rice straw under different temperatures, Biomass. Convers. Biorefinery 14 (12) (2022) 12775–12783.
[25] M. Keiluweit, P.S. Nico, M.G. Johnson, et al., Dynamic molecular structure of plant biomass-derived black carbon (biochar), Environ. Sci. Technol. 44 (2010) 1247–1253.
[26] Z. Ma, Y. Yang, Q. Ma, et al., Evolution of the chemical composition, functional group, pore structure and crystallographic structure of bio-char from palm kernel shell pyrolysis under different temperatures, J. Anal. Appl. Pyrolysis 127 (2017) 350–359.
[27] W.T. Li, B.H. Chai, M.J. Wang, Characterization of pyrolytic carbonization properties of different household waste fractions and pyrolysis char Fourier infrared spectroscopy, Adv. N. Renew. Energy 8 (01) (2020) 22–27.
[28] G. Imwinkelried, C.S. Fermanelli, M.A. Teruel, et al., Comprehensive analysis of soybean residues pyrolysis products, J. Anal. Appl. Pyrolysis 177 (2024).
[29] Y.F. Sun, C. Li, S. Zhang, et al., Pyrolysis of soybean residue: Understanding characteristics of the products, Renew. Energy 174 (2021) 487–500.
[30] W.C. Choi, H.D. Yun, J.Y. Lee, Mechanical properties of mortar containing bio-char from pyrolysis, J. Korea Inst. Struct. Maint. Insp. 13 (3) (2012) 67–74.
[31] A. Danish, M.A. Mosaberpanah, Influence of cenospheres and fly ash on the mechanical and durability properties of high-performance cement mortar under different curing regimes, Constr. Build. Mater. 279 (2021).
[32] S. Gupta, H.W. Kua, C.Y. Low, Use of biochar as carbon sequestering additive in cement mortar, Cem. Concr. Compos. 87 (2018) 110–129.
[33] D. Cuthbertson, U. Berardi, C. Briens, et al., Biochar from residual biomass as a concrete filler for improved thermal and acoustic properties, Biomass. Bioenergy 120 (2019) 77–83.
[34] S. Praneeth, L. Saavedra, M. Zeng, et al., Biochar admixtured lightweight, porous and tougher cement mortars: mechanical, durability and micro computed tomography analysis, Sci. Total Environ. 750 (2021).

[35] K.H. Tan, X.J. Pang, Y.H. Qin, et al., Properties of cement mortar containing pulverized biochar pyrolyzed at different temperatures, Constr. Build. Mater. 263 (2020).
[36] D. Pedro, J.D. Brito, L. Evangelista, Mechanical characterization of high performance concrete prepared with recycled aggregates and silica fume from precast industry, J. Clean. Prod. 164 (2017) 939–949.
[37] C.H. Jiang, W.W. Guo, H. Chen, et al., Effect of filler type and content on mechanical properties and microstructure of sand concrete made with superfine waste sand, Constr. Build. Mater. 192 (2018) 442–449.
[38] J.P. Li, R. Huang, Z. Chen, et al., Utilization potential of aerated concrete block powder and coffee grounds ash in green-growing concrete, Materials 17 (12) (2024) 3027.
[39] R.A. Khushnood, S. Ahmad, L. Restuccia, et al., Carbonized nano/microparticles for enhanced mechanical properties and electromagnetic interference shielding of cementitious materials, Front. Struct. Civ. Eng. 10 (2) (2016) 209–213.
[40] C. Zhou, Z.Y. Zhen, X.Q. Kong, Effect of high performance polypropylene fibers on the mechanical properties of recycled concrete, Sci. Technol. Eng. 21 (1) (2021) 303–309.
[41] J.J. Tang, C.C. Pei, Orthogonal method to analyze the tensile and flexural compression ratio of recycled concrete, Pearl River 40 (11) (2019) 68–71.
[42] J.B. Wang, H.X. Xu, D.Y. Xu, et al., Accelerated carbonation of hardened cement pastes: Influence of porosity, Constr. Build. Mater. 225 (2019) 159–169.
[43] B.W. Jo, M.A. Sikandar, S. Chakraborty, et al., Investigation of the acid and sulfate resistance performances of hydrogen-rich water based mortars, Constr. Build. Mater. 137 (2017) 1–11.
[44] Y.Q. Jia, H. Li, X.L. He, et al., Effect of biochar from municipal solid waste on mechanical and freeze–thaw properties of concrete, Constr. Build. Mater. 368 (2023).
[45] G. Murali, L.S. Wong, A comprehensive review of biochar-modified concrete: mechanical performance and microstructural insights, Constr. Build. Mater. 425 (2024).
[46] L. Qing, H. Zhang, Z. Zhang, Effect of biochar on compressive strength and fracture performance of concrete, J. Build. Eng. 78 (2023).
[47] D.D. Zhao, J.M. Williams, Z.Z. Li, et al., Hydration of cement pastes with calcium carbonate polymorphs, Cem. Concr. Res. 173 (2023) 107270.
[48] L.F. Morales, K. Herrera, J.E. López, et al., Use of biochar from rice husk pyrolysis: assessment of reactivity in lime pastes, Heliyon 7 (11) (2021) e08423.
[49] M.H. Javed, M.A. Sikandar, W. Ahmad, et al., Effect of various biochars on physical, mechanical, and microstructural characteristics of cement pastes and mortars, J. Build. Eng. 57 (2022).
[50] R. Mrad, G. Chehab, Mechanical and microstructure properties of biochar-based mortar: an internal curing agent for PCC, Sustainability 11 (9) (2019) 2491.